ELSEVIER

Contents lists available at ScienceDirect

Chemical Engineering Journal

journal homepage: www.elsevier.com/locate/cej



A biodegradable cellulose-based ionic conductor for sustainable and high-safety quasi-solid-state sodium batteries

Yuejing Zeng ^a, Rong Tang ^a, Minghui Chen ^a, Yaqi Zhang ^a, Wei Li ^a, Huiya Yang ^a, Ruilai Ye ^a, Xue Li ^{b,*}, Yang Yang ^{a,*}, Jinbao Zhao ^{a,*}

ARTICLE INFO

Keywords: Cellulose High safety Quasi-solid-state electrolyte Biodegradability

ABSTRACT

Solid-state sodium-ion batteries (SIBs) are promising for the next-generation power sources due to high energy density and safety. However, conventional solid-state electrolytes struggle with ionic conductivity, interfacial compatibility and manufacturability, impeding their commercial applications. Herein, a biodegradable Na⁺-infused cellulose-based quasi-solid electrolyte (CMC/S-Na QSE) with fast ion transfer kinetics and excellent interfacial stability is developed. Through a controlled sulfonation treatment, the breaking of high-crystalline cellulose chains is achieved, thereby creating engineered molecular channels for efficient Na⁺ ion conduction (2.1 \times 10 $^{-4}$ S cm $^{-1}$ at room temperature). CMC/S-Na QSE also exhibits high Na⁺ transference number (0.88) and wide electrochemical stability window (4.85 V vs Na⁺/Na), ensuring compatibility with Na-metal anodes and various SIBs cathodes. Consequently, CMC/S-Na QSE achieves long-term performance in pouch full-cells for over 250 cycles, highlighting its exceptional practicality. Importantly, retaining inherent biodegradability, mechanical strength, and thermal stability of cellulose, the CMC/S-Na QSE offer potential for developing sustainable and high-safety solid-state SIBs.

1. Introduction

The rapid development of modern society and growing demand for sustainable energy have fueled interest in safe and eco-friendly energy storage technologies [1,2]. Sodium-ion batteries (SIBs) have emerged as promising alternative to Lithium-ion batteries (LIBs), due to their low cost, resource abundance, and promising electrochemical performance [3-7]. However, the progress of SIBs is hindered by challenges associated with traditional liquid electrolytes, such as flammability, leakage and environmental risks [8-10]. Solid-state-electrolytes (SSEs) offer a safer and more stable option. Among them, solid polymer electrolytes (SPEs) are attractive due to their lightweight nature, flexibility, and improved interfacial compatibility compared to brittle inorganic solidstate electrolytes [11-14]. However, SPEs also suffer from poor mechanical strength and low ionic conductivity at room temperature [15,16]. Ion transport in SPEs typically relies on the movement of polymer segments, which is hindered by crystallinity at ambient temperatures [17]. Various strategies have been explored to enhance SPE performance, including addition of inorganic fillers [18], block copolymers [19], single-ion conductors [20], and cross-linking networks [21]. Yet, achieving a balance between conductivity, ion transference, and sustainability remains challenging.

Therefore, it is imperative to radically transform the traditional structure and ion-transport mechanism of SPEs. Cellulose, the most abundant natural polymer, offers biodegradability, and environmental friendliness. Its polar oxygen-containing groups can coordinate with cations, enabling ion transport [22]. However, strong hydrogen bonding between cellulose chains restricts segmental motion and limits ionic conductivity. In 2021, a pioneering work by Hu et al. incorporated Cu²⁺ coordination with cellulose chains to enlarge the spacing between cellulose molecular chains, achieving ultra-fast Li⁺ conduction [23]. Moreover, Tian et al. introduces CH₂COO⁻ groups in cellulose acetate (CLA) to reduce hydrogen bonding and enhance Li⁺ mobility [24]. Therefore, breaking the packed cellulose chains and functional group modification are crucial to establish molecular channels for fast ion diffusion. Nevertheless, using metals like Cu may compromise

E-mail addresses: 438616074@qq.com (X. Li), yangyang419@xmu.edu.cn (Y. Yang), jbzhao@xmu.edu.cn (J. Zhao).

 ^a State Key Laboratory of Physical Chemistry of Solid Surfaces, Collaborative Innovation Center of Chemistry for Energy Materials, State-Province Joint Engineering Laboratory of Power Source Technology for New Energy Vehicle, College of Chemistry and Chemical Engineering, Xiamen University, Xiamen, 361005, China
^b National and Local Joint Engineering Research Center of Lithium-ion Batteries and Materials Preparation Technology, Faculty of Metallurgical and Energy Engineering, Kunming University of Science and Technology, Kunming, 650093, China

^{*} Corresponding authors.

biodegradability and excessive modification risks may weaken mechanical strength.

In this work, we explore a facile in-situ sulfonation method to create a flexible and biodegradable ionic-conductor for high-safety quasi-solidstate SIBs. The mild sulfonation treatment enables controlled modification, disrupting the dense cellulose structure while preserving mechanical strength. The introduced sulfonate groups mitigate the hydrogen bonding and act as efficient conduction sites, promoting directional Na⁺ transport and achieving a high transference number. With the aid of oxygen-containing groups, sulfonate sites, and bound solvents, Na⁺ ions move smoothly through well-structured conduction channels (Fig. 1a). The resulting Na+-infused cellulose-based quasi-solid electrolyte (CMC/S-Na QSE) demonstrates high ion conductivity (2.1 imes10⁻⁴ S cm⁻¹), impressive Na⁺ transference number of 0.88 and wide electrochemical window of 4.85 V (vs. Na⁺/Na) at ambient temperature. It also exhibits exceptional compatibility with Na metal anode, maintaining stable Na-plating/stripping of lifespan exceeding 1000 h. Furthermore, CMC/S-Na QSE delivers superior safety features, ensuring reliable battery stability even under extreme conditions like acupuncture. Most importantly, the hard carbon//NaNi_{1/3}Fe_{1/3}Mn_{1/3}O₂ (HC// NFM) pouch full battery using CMC/S-Na QSE achieves preferable cycling stability with 89 % capacity retention after 250 cycles. These results underscore the potential of this innovative cellulose-based QSE as a promising candidate for the next generation high-performance SIBs.

2. Results and discussion

2.1. Fabrication and characterization of CMC/S-Na QSE

The cellulose-based quasi-solid electrolyte was prepared via a vacuum filtration method combined with in-situ sulfonation treatment (Scheme S1). Briefly, a dense cellulose membrane (CMC) was obtained by vacuum filtration of a mixed suspension containing cellulose nanowhisker (CNC) and micro-fibrillated cellulose (MFC), followed by pressing between two filter membranes at 10 MPa for 10 min. The CMC membrane underwent a sulfonation treatment for 2 weeks, yielding a cellulose membrane with sulfonate groups and loosened molecular chains (CMC/S) with thickness of approximately 80 µm. Finally, Na⁺infused cellulose-based quasi-solid electrolyte (CMC/S-Na QSE) was obtained by soaking CMC/S in an electrolyte containing NaPF6 in nonaqueous solvents. Repeated pressing and wiping of the absorbed solvent and evaporating solvent were conducted until all free-solvent were thoroughly removed for CMC/S-Na QSE prior to use. A representative CMC/S-Na QSE (6 cm × 6 cm) is shown in Fig. 1b, highlighting its remarkable ease of production. The evolution of cellulose structure during preparation was monitored using two-dimensional small-angle X-ray scattering (SAXS) and XRD. XRD analysis (Fig. S1) and SAXS results (Fig. S2a) reveal that pristine cellulose exhibits a typical crystalline structure of cellulose I_B polymorph, characterized by diffraction peaks like (002) and (101) (Fig. 1c) [25]. After sulfonation treatment, the

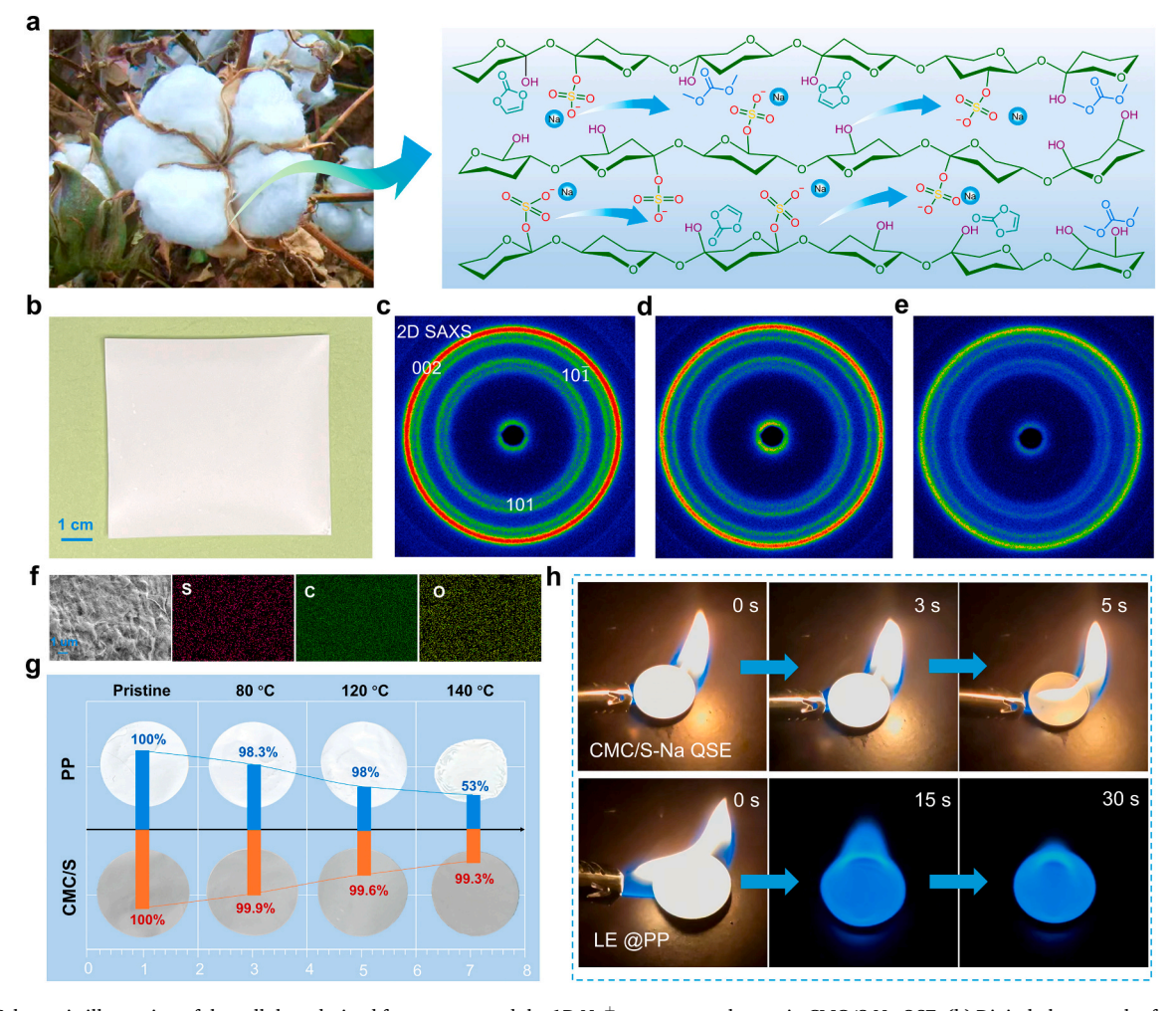


Fig. 1. (a) Schematic illustration of the cellulose derived from cotton and the 1D Na⁺ transport pathways in CMC/S-Na QSE. (b) Digital photograph of a 6 cm × 6 cm CMC/S-Na QSE. The 2D small-angle diffraction patterns of the CMC (c), CMC/S (d) and CMC/S-Na (e) membranes. (f) The SEM images of CMC/S membrane and its EDS mapping of C, O and S element. (g) Thermal stability of CMC/S membrane and PP separator at different temperatures for 30 mins. (h) Flammability measurement for CMC/S-Na QSE and PP separator carrying liquid electrolyte.

crystallinity of cellulose decrease from 96 % to 73 %, as evidenced by the blurring of 2D SAXS stripes (Fig. 1d) and fitting results (Fig. S2b-2c), suggesting partial disruption of tightly packed cellulose chains and reduced hydrogen bonding [26]. The crystallinity further decreased after Na $^+$ incorporation (Figs. 1e and S2d), enhancing Na $^+$ migration and confirming the effectiveness of the preparation process.

Scanning electron microscope (SEM) images and energy dispersive spectroscopy (EDS) mapping of cellulose membranes reveal a smooth surface morphology with porosity of 9.3 % and the uniform distribution of elements C, O and S (Figs. 1f and S3). The detection of S element in EDS mapping confirms the existence of sulfonate groups, supported by XPS (X-ray photoelectron spectroscopy) results (Fig. S4). FT-IR (Fourier transform infrared spectroscopy) patterns (Fig. S5a-b) and Raman analysis [27] (Fig. S6a) also identify sulfonate groups, while elemental analysis (Table S1) indicates a slight increase in S content, validating the successful sulfonation treatment. Superior mechanical strength and thermal stability are essential for QSEs to prevent dendrite growth and ensure battery safety. The stress-strain curve for CMC/S-Na QSE depicts excellent mechanical strength compared to typical glass fibres (Fig. S7). Fig. 1g displays that while PP separator shrinks violently at 140 °C, the CMC/S membrane remains stable, demonstrating exceptional thermal stability. Combustion experiments further confirm the safety of the CMC/S-Na QSE. Unlike the PP separator with liquid electrolyte, which burns for over 30 s, the CMC/S-Na QSE is hard to maintain continuous

burning (Fig. 1h). These results collectively highlight the superior mechanical performance and thermal stability of CMC/S-Na QSE, laying a solid foundation for its outstanding role in batteries. Compared to liquid electrolytes (LE), CMC/S-Na QSE shows distinct interactions between solvent molecules and cellulose molecular chains, as evidenced by variations in carbonyl groups in FT-IR and Raman results (Figs. S5c-d and S6b). Thermogravimetry (TG) analysis (Fig. S8) show while CMC/S-Na QSE decomposes slightly earlier than pristine CMC/S membrane, it maintains good thermal stability and mechanical strength, aligning with previous results.

2.2. Na+ conduction in CMC/S-Na QSE

Molecular dynamics (MD) simulations were performed to investigate the coordination environment of CMC/S-Na QSE. The radial distribution function (RDF) analysis exhibits a prominent peak at approximately 0.2 nm, representing primary solvation shell of Na $^+$ (Fig. S9) [8,28 $^-$ 30]. In LE, Na $^+$ primarily interacts with PF $_6$ $^-$, EC, and DMC, with coordination number of 2.16, 1.47, and 1.46, respectively (Fig. 2a, d). Conversely, in CMC/S-Na QSE, Na $^+$ also exhibits interactions with -OH, except for PF $_6$, EC, and DMC, with coordination number of 0.69, 2.69, 0.54 and 0.17. (Fig. 2b, d). The -OH groups in CMC/S-Na QSE also exhibit a high affinity for PF $_6$, EC, and DMC (Fig. 2c), aligning with Raman and FT-IR analysis, confirming the existence of bound solvents. These results

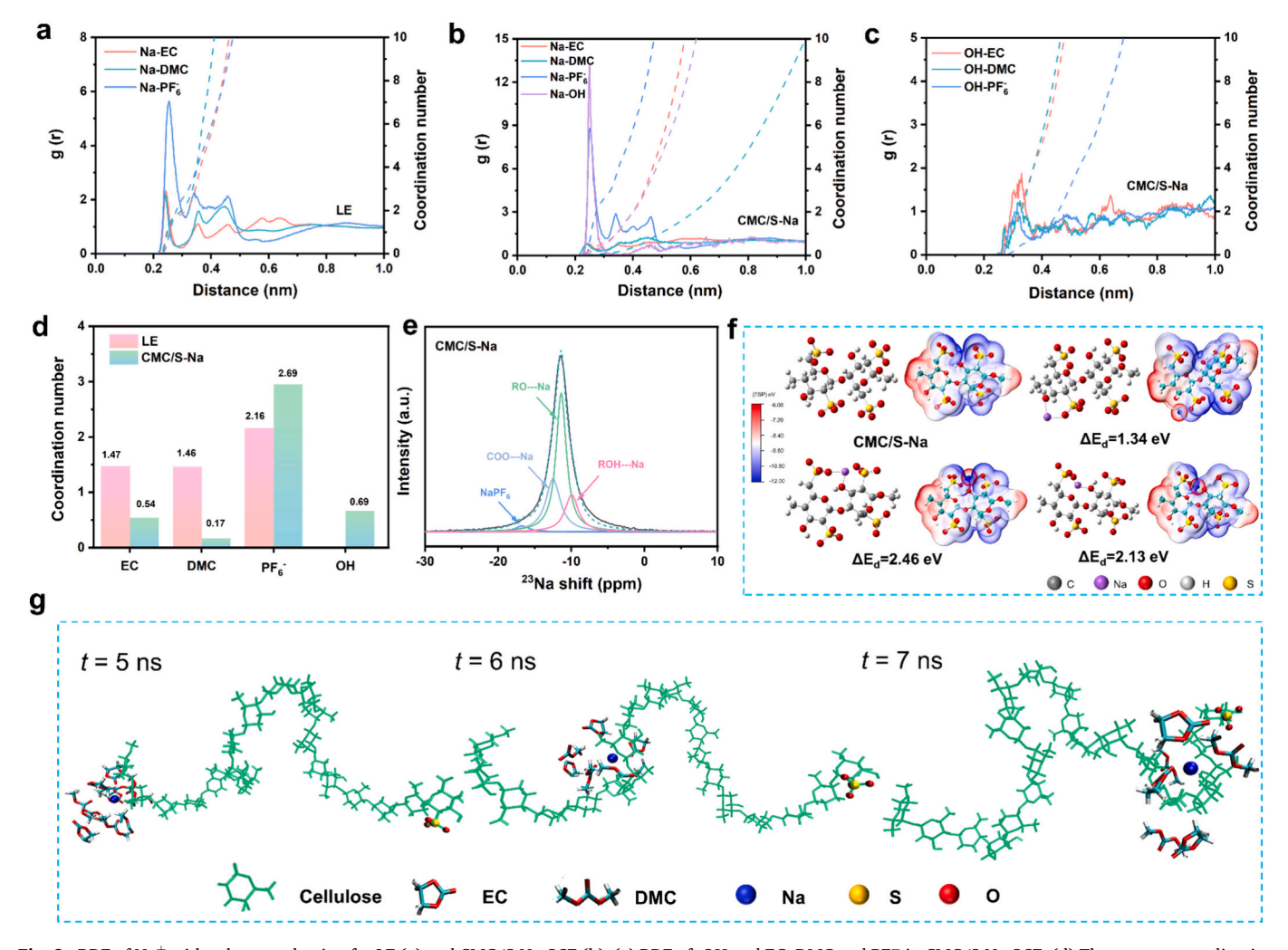


Fig. 2. RDF of Na $^+$ with solvent and anion for LE (a) and CMC/S-Na QSE (b). (c) RDF of -OH and EC, DMC and PF $_6^-$ in CMC/S-Na QSE. (d) The average coordination number of solvent and anion of Na $^+$ in CMC/S-Na QSE and LE. (e) The 23 Na solid-state NMR spectra for CMC/S-Na QSE. (f) MESP illustration for CMC/S-Na with Na $^+$ and corresponding dissociation energy of CMC/S-Na bound to Na $^+$. (g) The simulated structural snapshots from MD simulations of moving Na $^+$ transporting in CMC/S-Na QSE during 5–7 ns.

demonstrate the distinct solvation structure of CMC/S-Na QSE compared to LE and the importance of oxygen-containing functional groups in ion migration. $^{23}\mathrm{Na}$ solid-state nuclear magnetic resonance (NMR) spectroscopy (Figs. 2e and S10) further show that, Na $^+$ coordinates not only with PF $_6^-$ but also with oxygen-containing functional groups such as hydroxyl (ROH-), alkoxide (RO-), and structural solvents [23,31]. These structural solvent assist Na $^+$ in continuous conduction along oxygen-containing functional groups and directional conduction sites of sulfonate groups on the cellulose chain. Figs. S11 and 2f further show that Na $^+$ has stronger coordination with -SO $_3^-$ and -OH groups indicating the critical role of sulfonated groups in Na $^+$ migration.

The molecular electrostatic potential (MESP) analysis reveals that negative charges in CMC/S-Na QSE are primarily located at SO_3^- and -OH position, facilitating coordination with Na^+ . Upon coordination, positive charges accumulate around Na^+ , highlighting strong interaction. Sulfonate groups are widely recognized as efficient conduction sites for single-ion conductors, which significantly enhancing the directional conduction of Na^+ and enables the attainment of high Na^+ transference number [12]. Therefore, Fig. 2g depicts the simulated swift migration of Na^+ along cellulose chains, with corresponding simulation box in Fig. S12. The simulations reveal that Na^+ transport rapidly along the cellulose molecular chain, while the cellulose skeleton remains nearly stationary. This decoupling of ion displacement from the cellulose molecular chain facilitates efficient Na^+ migration. This ion

migration model is achieved with the assistance of multiple Na—O coordination, directional conduction sites of functionalized sulfonate groups and a small number of bound solvent molecules, enabling CMC/S-Na QSE to reach high ion conductivity and Na⁺ transference number.

2.3. Application of CMC/S-Na QSE in sodium batteries

Electrochemical impedance spectroscopy (EIS) of CMC/S-Na OSE was performed across temperature ranging from 20 to 80 °C, revealing a temperature-sensitive ionic conductivity pattern consistent with the Arrhenius equation [32] (Figs. 3a and S13). At room temperature, CMC/ S-Na QSE exhibits high ionic conductivity of 2.1×10^{-4} S cm⁻¹. Linear sweep voltammetry (LSV) shows significantly enhanced electrochemical stability and a wider electrochemical window compared to LE (Fig. 3b). Density functional theory (DFT) calculations reveal the high electrochemical stability of CMC/S-Na QSE linked to the values of highest occupied molecular orbital (HOMO) with -6.39 eV and -6.93 eV for CMC/S and CMC (Fig. 3e). The superior antioxidant property primarily arises from the electron-withdrawing nature of oxygen-containing functional groups on cellulose chains. The Na⁺ transference number for CMC/S-Na QSE is 0.88, significantly higher than that of LE (0.45) (Figs. 3c and S14). This performance is due to the efficient Na⁺ migration channels enabled by oxygen-containing functional groups and functionalized sulfonate groups. These results indicate that CMC/S-Na

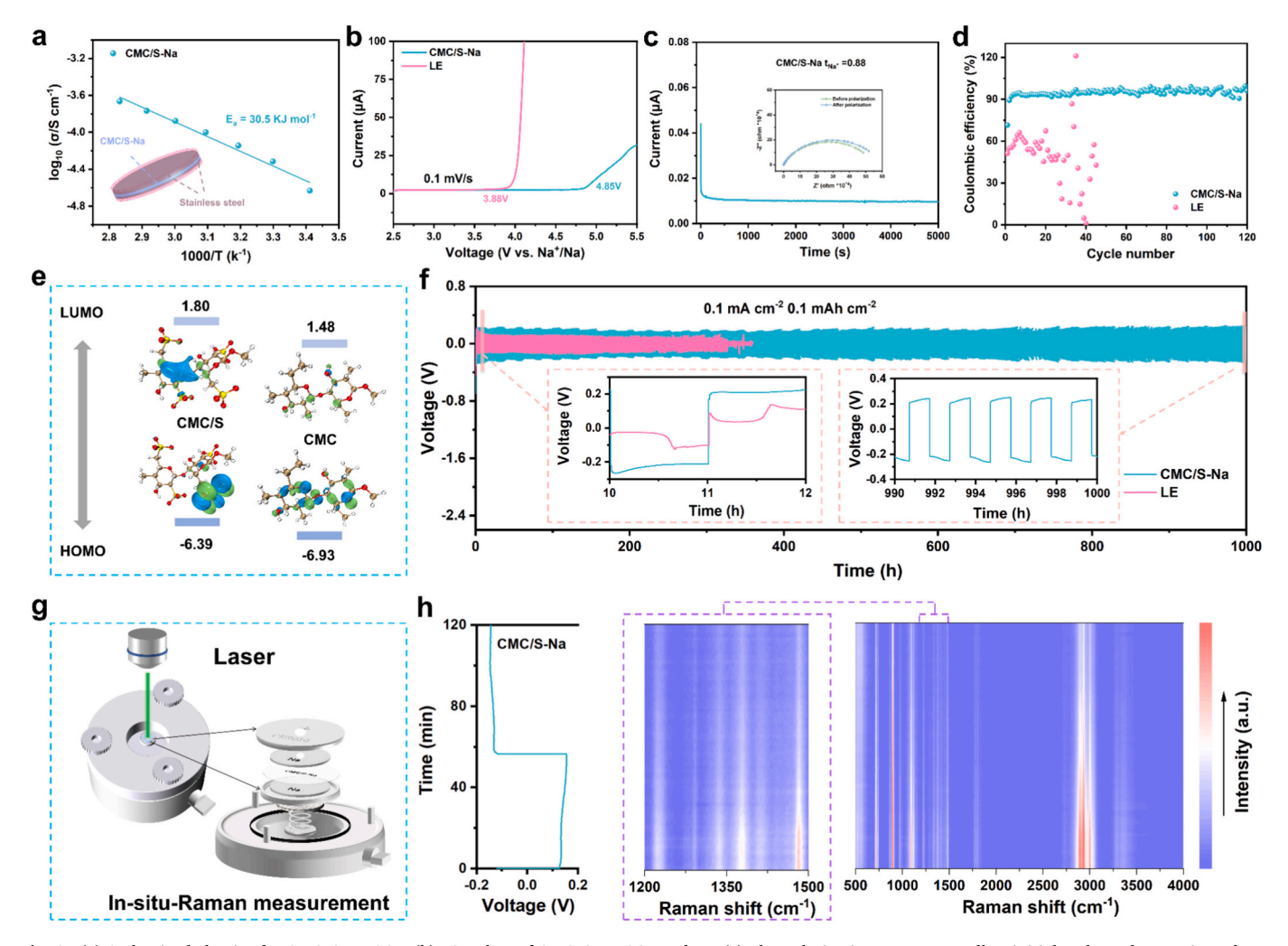


Fig. 3. (a) Arrhenius behavior for CMC/S-Na QSE. (b) LSV plots of CMC/S-Na QSE and LE. (c) The polarization curves as well as initial and steady state impedance program of Na//Na cell for CMC/S-Na QSE. (d) The cycling performance of Na//AlC half-cell in CMC/S-Na QSE and LE. (e) The HOMO and LUMO energy levels of CMC and CMC/S. (f) The cycling performance of Na//Na symmetric cell at 0.1 mA cm⁻² and 0.1 mAh cm⁻² for CMC/S-Na QSE and LE. The in-situ Raman measurement of Na//Na battery of CMC/S-Na QSE (g) and corresponding result at second cycling (h).

QSE offers outstanding electrochemical stability and high ionic conductivity, making it compatible with sodium metal and high-voltage cathode materials.

To evaluate the compatibility of CMC/S-Na QSE with sodium metal, Na//Al@C half cells were fabricated. CMC/S-Na QSE exhibits a higher initial Coulombic efficiency (71.4 %) than LE (52.3 %), and maintains coulombic efficiency of 95 % over 120 cycles, indicating restrained interfacial reactions (Fig. 3d). It also supports stable Na deposition/stripping with steady polarization voltage for 1000 h at 0.1 mA cm⁻² and 0.1 mAh cm⁻², outperforming LE (Fig. 3f), and perform well at higher current densities (Fig. S15). In-situ Raman spectroscopy of CMC/S-Na QSE were collected in Na//Na symmetrical cells to further characterize its structural stability during electrochemical cycling (Fig. 3g). There are no observable peak shifts during the Na deposition/stripping

cycles, underscoring the high electrochemical stability of CMC/S-Na QSE (Fig. 3h). Overall, CMC/S-Na QSE demonstrates excellent compatibility with sodium metal.

Benefiting from its outstanding interfacial and structural stability, the Na//NFM cell using CMC/S-Na QSE exhibits good cycling performance at a high cut-off voltage of 4.3 V at 0.1C ($1C = 150 \text{ mAh g}^{-1}$) (Fig. 4a). Simultaneously, Na//NFM cell with cut-off voltage of 4.0 V was also assembled, showing stable cycling after 100 cycles at 0.1C (Fig. 4b). XPS analysis reveals that the NFM surface cycled in CMC/S-Na QSE has higher NaF content, (Fig. 4e) than in LE, originating from the decomposition of PF₆ [34], while the O 1 s spectrum (Fig. 4f) shows similar compositions for both electrolytes. Moreover, Na//NVP half-cell using CMC/S-Na QSE achieves a 93.1 % capacity retention after 500 cycles at 1C ($1C = 100 \text{ mAh g}^{-1}$) (Fig. 4c), and perform better than LE at

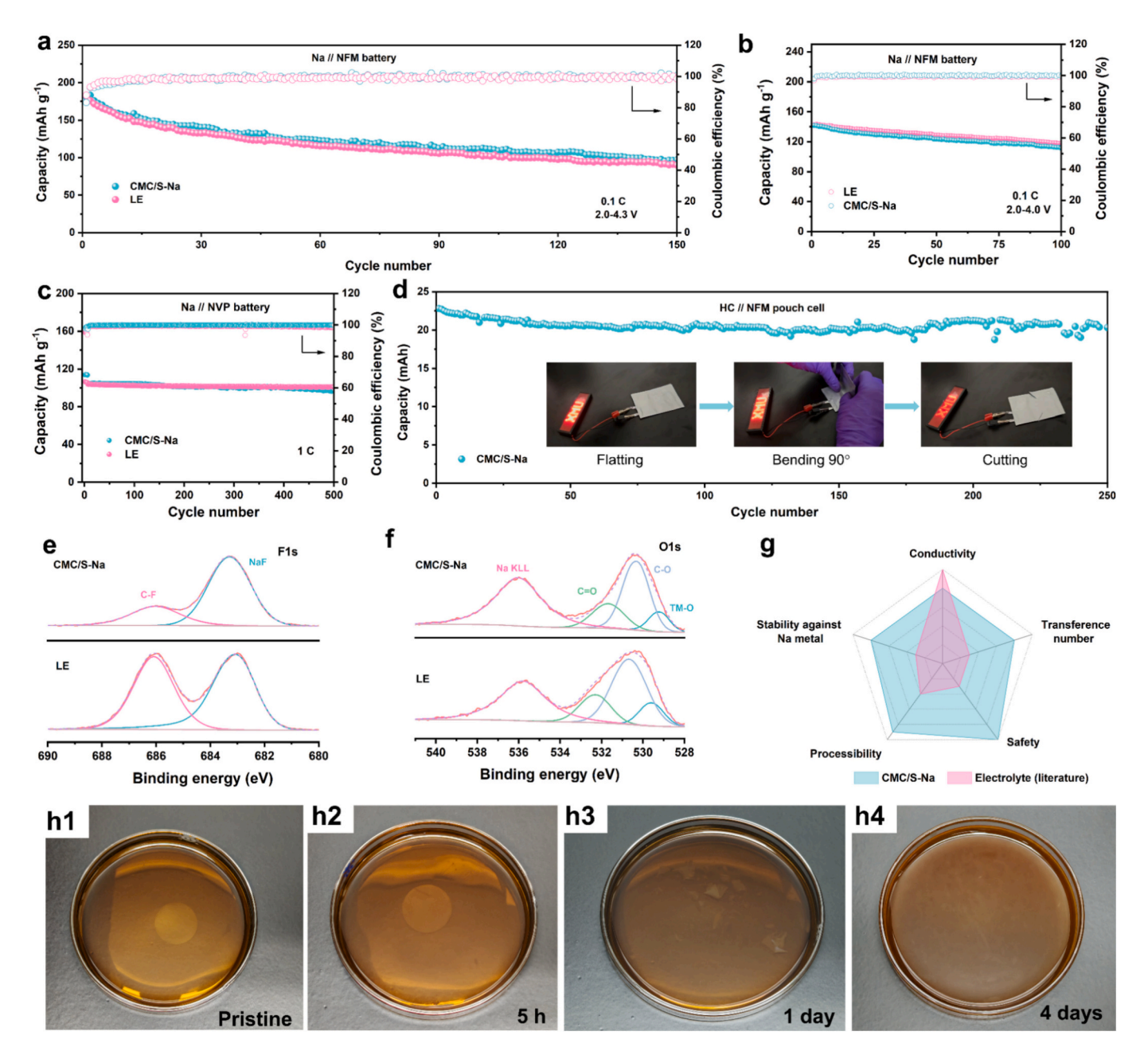


Fig. 4. Cycling performance of Na//NFM half-cells at 0.1C under 4.3 V (a) and 4.0 V (b) for CMC/S-Na QSE and LE. (c) Cycling performance of Na//NVP half-cell at 1C for CMC/S-Na QSE at 0.1C (insets show the flexibility and security of pouch cell under various harsh conditions). The XPS spectra of F 1s (e) and O 1s (f) for NFM cathode from Na//NFM cycled 10 cycles in CMC/S-Na QSE and LE. (g) The spider chart for performance of CMC/S-Na QSE and LE in literature [23,24,28,33]. (h1-h4) Optical photographs of decomposition process of CMC/S membrane in the classic Fehling reagent.

0.1C (Fig. S16). Furthermore, HC//NFM full cells in coin-type with CMC/S-Na QSE were also assembled (Fig. S17), while a soft-packaged HC//NFM full cell (3 cm \times 3 cm) employing CMC/S-Na QSE exhibits preferable cycling stability, with over 89 % capacity retention after 250 cycles at 0.1C (Figs. 4d and S18). The soft-packaged full-cell demonstrates excellent flexibility, maintaining LED brightness even after 90° bending or cutting, confirming the reliability of CMC/S-Na QSE. It can be seen that the pouch cells in this work exhibit clear advantages in both capacity and cycling performance (Table S2).

It is noteworthy that CMC/S membrane is biodegradable, as its anhydroglucose-based structure can be broken down by cellulase. The membrane almost completely degrades after just 4 days in a cellulase medium, implying a satisfactory degradation rate (Fig. 4h1-4h4). This makes it a promising eco-friendly QSE, aiding in battery recycling and disposal. Generally, CMC/S-Na QSE crafted from biodegradable and environmentally friendly cellulose, offers several key attributes, including fast ion conductivity, high transference numbers, good stability with sodium metal, ease of processing, and enhanced safety (Fig. 4g).

In-situ XRD was employed to investigate the structural evolution of NFM and NVP cathodes in LE and CMC/S-Na QSE. During initial charging in Na//NFM half-cell, a solid-solution reaction of the O3 phase occurs, resulting in expansion along the c-axis and contraction along the

a-axis. Subsequently, the splitting of peaks (003) and (006), along with a weakening of the (104) peak intensity, indicates a two-phase reaction between O3 and P3 phase. The transition to the P3 phase completes when (104) peak disappears, accompanied by continuous shifts of P3 phase peaks until 4.0 V, where a monophasic solid-solution reaction occurs. During discharge, a reverse transformation from P3 to O3 phase occurs [35]. NFM in CMC/S-Na QSE exhibits better structural stability, with smaller (003) peak shift (0.026°) compared to (0.094°) in LE (Fig. 5a-b). Furthermore, the c-axis variation of NFM in CMC/S-Na QSE is 0.927, less than 1.038 in LE, indicating less volume expansion and irreversible structural collapse (Figs. 5c-d and S19). In HC//NFM pouch full-cell, the (003) peak shift is smaller in CMC/S-Na QSE (0.021) than in LE (0.029), suggesting better structural integrity, correlating with its cycling stability (Fig. 5e-g). For Na//NVP half-cell, XRD reveals that during charging, Na₃V₂(PO₄)₃ phase undergoes a two-phase process transition to NaV₂(PO₄)₃ phase, with fully reversibility upon discharge (Fig. S20) [36]. NVP exhibits a similar phase transition process in both CMC/S-Na QSE and LE, indicating a similar structural evolution. The safety performance of batteries utilizing CMC/S-Na QSE was assessed under mechanical abuse, through needle penetration tests. Such abuse often causes internal short circuit, risking thermal runaway [37]. A needle penetration experiment was conducted on 430 mAh fullycharged battery, with a forward-looking infrared (FLIR) camera

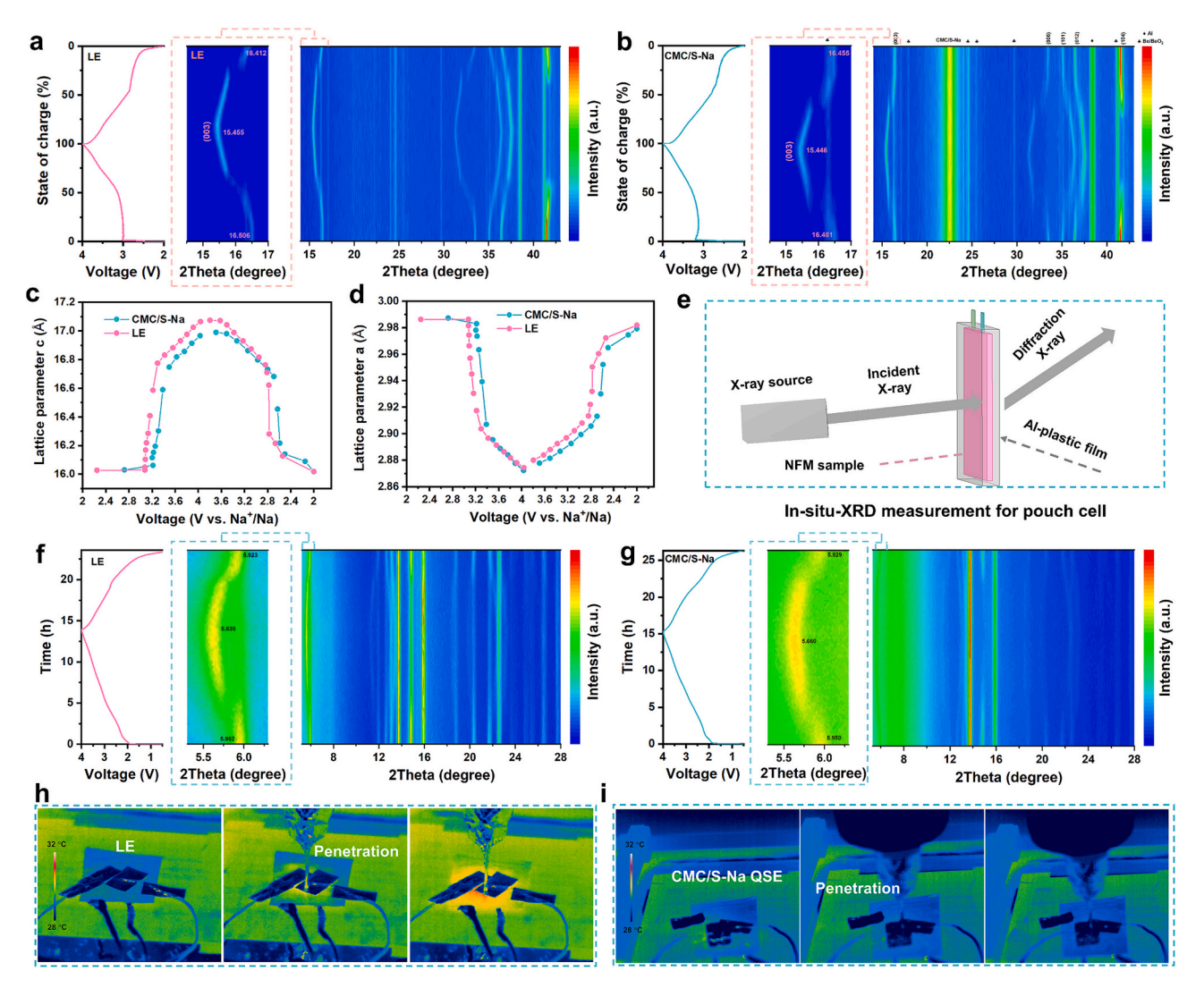


Fig. 5. In-situ XRD result of Na//NFM half-cell at initial cycle of LE (a) and CMC/S-Na QSE (b). The corresponding change of lattice parameter c (c) and a (d) for LE and CMC/S-Na QSE. (e) The in-situ XRD measurement for HC//NFM pouch cell. In-situ XRD result of HC//NFM pouch full-cell at initial cycle of LE (f) and CMC/S-Na QSE (g). FLIR images of the pouch-cell with LE (h) and CMC/S-Na QSE (i) under acupuncture experiment.

monitoring real-time temperature changes. While thermal runaway did not occur due to relatively low capacity, significant heat accumulation and temperature rise were observed in LE-based battery (Fig. 5h). In contrast, the battery incorporating CMC/S-Na QSE demonstrates minimal temperature variation (Fig. 5i), indicating its ability to prevent rapid temperature increase and enhance battery safety under extreme conditions.

3. Conclusions

In summary, we have developed an innovative biodegradable and flexible cellulose-based quasi-solid electrolyte (CMC/S-Na QSE) for high-safety sodium batteries, utilizing a straightforward and reproducible synthesis method. The controlled sulfonation treatment in a weaklyacid buffer creates molecular channels for rapid Na⁺ ion conduction $(2.1 \times 10^{-4} \, \mathrm{S \, cm^{-1}}$ at room temperature) by breaking high-crystalline cellulose chains and incorporating sulfonate groups. Experimental results and molecular dynamics (MD) simulations illustrate Na⁺ conduction along oxygen-containing functional groups and sulfonate groups on cellulose chain supported by structural solvent on the basis of loosened cellulose molecular chains, CMC/S-Na OSE also exhibits high Na⁺ transference number (0.88), broad electrochemical stability window (4.85 V) and excellent processability, benefiting from regulated Na+ coordination environment. Furthermore, CMC/S-Na QSE delivers outstanding safety features, ensuring reliable battery stability under mechanical abuse like acupuncture. In pouch full-cell HC//NFM with CMC/S-Na QSE, it achieves preferable cycling stability with 89 % capacity retention after 250 cycles. Furthermore, the biodegradable nature of CMC/S-Na QSE opens avenues for advanced, cost-effective, and sustainable sodium battery solutions.

4. Experiment section

The specific experimental information is provided in the supplementary material.

CRediT authorship contribution statement

Yuejing Zeng: Writing – original draft, Software, Methodology, Investigation, Formal analysis, Data curation, Conceptualization. Rong Tang: Writing – review & editing, Software, Data curation. Minghui Chen: Writing – review & editing, Data curation. Yaqi Zhang: Methodology. Wei Li: Writing – review & editing. Huiya Yang: Writing – review & editing. Ruilai Ye: Writing – review & editing. Xue Li: Writing – review & editing, Supervision, Funding acquisition. Yang Yang: Writing – review & editing. Supervision, Project administration, Funding acquisition. Jinbao Zhao: Writing – review & editing, Supervision, Resources, Project administration, Funding acquisition.

Declaration of competing interest

The authors declare that they have no known competing financial interests or personal relationships that could have appeared to influence the work reported in this paper.

Acknowledgments

This work is supported by National Natural Science Foundation of China (22021001), Fundamental Research Funds for the Central Universities (20720220073), Fujian Industrial Technology Development and Application Plan (202210002), Yunnan Key Research and Development Program (202403AA080018), Yunnan Engineering Research Center Innovation Ability Construction and Enhancement Projects (2023-XMDJ-00617107), Scientific and Technological Project of Yunnan Precious Metals Laboratory (YPML-20240502015), Natural Science Foundation of Yunnan Province (202401AS070646). The

numerical calculations in this paper have been done on Hefei advanced computing center.

Appendix A. Supplementary data

Supplementary data to this article can be found online at https://doi.org/10.1016/j.cej.2025.168883.

Data availability

Data will be made available on request.

References

- [1] M. Yu, N. Chandrasekhar, R.K.M. Raghupathy, K.H. Ly, H. Zhang, E. Dmitrieva, C. Liang, X. Lu, T.D. Kuhne, H. Mirhosseini, I.M. Weidinger, X. Feng, A high-rate two-dimensional polyarylimide covalent organic framework anode for aqueous Znion energy storage devices, J. Am. Chem. Soc. 142 (2020) 19570–19578, https:// doi.org/10.1021/jacs.0c07992.
- [2] N. Yue, S. Umer, R. Subramaniam, W.Y. Teoh, C. Yang, Emerging metal–polymer frameworks: structure, applications, and perspectives, Adv. Funct. Mater. n/a (n. d.) 2425506. https://doi.org/10.1002/adfm.202425506.
- [3] C. She, X. Shi, J. Zhou, Z. Zhu, K. Lu, Z. Zheng, Y. Zhu, A ZIF-8-enhanced PVDF/ PEO blending polymer gel membrane for quasi-solid-state Na-S batteries with long cycling lifespan, Chem. Eng. J. 494 (2024) 153119, https://doi.org/10.1016/j. cei.2024.153119.
- [4] W. Yuan, M. Ding, J. Weng, T. Xue, M. Xie, P. Zhang, J. Mu, P. Zhou, Composite electrolyte membrane with continuous Na+ transport for high-performance quasisolid-state sodium batteries, Chem. Eng. J. 514 (2025) 163142, https://doi.org/ 10.1016/j.cej.2025.163142.
- [5] S. Li, H. Liu, H. Qiu, X. He, W. Fan, W. Wang, J. Nan, An electrolyte design strategy for commercial all-climate pouch sodium-ion batteries, Chem. Eng. J. 505 (2025) 159102, https://doi.org/10.1016/j.cej.2024.159102.
- [6] P. Ma, Y. Zhang, W. Li, J. Luo, L. Wen, G. Tang, J. Gai, Q. Wang, L. Zhao, J. Ge, W. Chen, Tailoring alloy-reaction-induced semi-coherent interface to guide sodium nucleation and growth for long-term anode-less sodium-metal batteries, Sci. China Mater. 67 (2024) 3648–3657, https://doi.org/10.1007/s40843-024-3084-4.
- [7] X. Xiao, J. Li, X. Meng, J. Qiu, Sulfur-doped carbon-coated Fe0.95S1.05 nanospheres as anodes for high-performance sodium storage, Acta Phys. -Chim. Sin. 40 (2024) 2307006, https://doi.org/10.3866/PKU.WHXB202307006.
- [8] M. Liu, Z. Zeng, C. Gu, F. Ma, Y. Wu, Q. Wu, X. Yang, X. Chen, S. Cheng, J. Xie, Ethylene carbonate regulated solvation of triethyl phosphate to enable highconductivity, nonflammable, and graphite compatible electrolyte, ACS Energy Lett. 9 (2023) 136–144, https://doi.org/10.1021/acsenergylett.3c02414.
- [9] B. Pei, Z. Zheng, Z. Cao, G. Fang, J. Zhou, X. Cao, S. Liang, Manipulating interfacial chemistry of hard carbon anodes through single-atom catalysis and formation cycling towards fast-charging sodium-ion batteries, Sci. Bull. (2025), https://doi. org/10.1016/j.scib.2025.03.042.
- [10] H. Liu, T. Zhu, J. Liao, Z. Ma, X. Zuo, J. Nan, Rigid-flexible methyl cellulose/ polyvinylpyrrolidone hybrid nonporous membrane with high ionic transport for high performance sodium ion batteries, Chem. Eng. J. 503 (2025) 158471, https:// doi.org/10.1016/j.cej.2024.158471.
- [11] C. Sun, J. Liu, Y. Gong, D.P. Wilkinson, J. Zhang, Recent advances in all-solid-state rechargeable lithium batteries, Nano Energy 33 (2017) 363–386, https://doi.org/ 10.1016/j.nanoen.2017.01.028.
- [12] Y. Zeng, J. Yang, X. Shen, R. Li, Z. Chen, X. Huang, P. Zhang, J. Zhao, New UV-initiated lithiated-interpenetrating network gel-polymer electrolytes for lithium-metal batteries, J. Power Sources 541 (2022) 231681, https://doi.org/10.1016/j.jpowsour.2022.231681.
- [13] M. Akbar, I. Moeez, A.H. Umar Bhatti, Y.H. Kim, M. Kim, J.-Y. Kim, J. Jeong, J. H. Park, K.Y. Chung, Antimony-doped NASICON-type solid electrolyte with homogeneous sodium-ion flux for high-temperature solid-state sodium batteries, Chem. Eng. J. 517 (2025) 164300, https://doi.org/10.1016/j.cej.2025.164300.
- [14] H.-J. Liang, H.-H. Liu, J.-Z. Guo, X.-X. Zhao, Z.-Y. Gu, J.-L. Yang, X.-Y. Zhang, Z.-M. Liu, W.-L. Li, X.-L. Wu, Self-purification and silicon-rich interphase achieves high-temperature (70°C) sodium-ion batteries with nonflammable electrolyte, Energy Storage Mater. 66 (2024) 103230, https://doi.org/10.1016/j.ensm.2024.103230.
- [15] X. Cheng, J. Pan, Y. Zhao, M. Liao, H. Peng, Gel polymer electrolytes for electrochemical energy storage, Adv. Energy Mater. 8 (2018) 1702184, https://doi.org/10.1002/aenm.201702184.
- [16] X.-X. Zhao, X.-T. Wang, Z.-Y. Gu, J.-Z. Guo, J.-M. Cao, Y. Liu, J. Li, Z.-X. Huang, J.-P. Zhang, X.-L. Wu, Unlocking quasi-monophase behavior in NASICON cathode to drive fast-charging toward durable sodium-ion batteries, Adv. Funct. Mater. 34 (2024) 2402447, https://doi.org/10.1002/adfm.202402447.
- [17] R. Li, H. Hua, X. Yang, J. Tian, Q. Chen, R. Huang, X. Li, P. Zhang, J. Zhao, The deconstruction of a polymeric solvation cage: a critical promotion strategy for PEObased all-solid polymer electrolytes, Energy Environ. Sci. 17 (2024) 5601–5612, https://doi.org/10.1039/D4EE01188K.
- [18] W. Liu, N. Liu, J. Sun, P.-C. Hsu, Y. Li, H.-W. Lee, Y. Cui, Ionic conductivity enhancement of polymer electrolytes with ceramic nanowire fillers, Nano Lett. 15 (2015) 2740–2745, https://doi.org/10.1021/acs.nanolett.5b00600.

- [19] R. Bouchet, S. Maria, R. Meziane, A. Aboulaich, L. Lienafa, J.-P. Bonnet, T.N. T. Phan, D. Bertin, D. Gigmes, D. Devaux, R. Denoyel, M. Armand, Single-ion BAB triblock copolymers as highly efficient electrolytes for lithium-metal batteries, Nat. Mater. 12 (2013) 452–457, https://doi.org/10.1038/nmat3602.
- [20] Q. Ma, H. Zhang, C. Zhou, L. Zheng, P. Cheng, J. Nie, W. Feng, Y. Hu, H. Li, X. Huang, L. Chen, M. Armand, Z. Zhou, Single lithium-ion conducting polymer electrolytes based on a super-delocalized polyanion, Angew. Chem. Int. Ed. 128 (2016) 2567–2571, https://doi.org/10.1002/ange.201509299.
- [21] X. Shen, L. Peng, R. Li, H. Li, X. Wang, B. Huang, D. Wu, P. Zhang, J. Zhao, Semi-interpenetrating network-structured single-ion conduction polymer electrolyte for lithium-ion batteries, ChemElectroChem 6 (2019) 4483–4490, https://doi.org/10.1002/celc.201901045.
- [22] Y. Fu, L. Yang, M. Zhang, Z. Lin, Z. Shen, Recent advances in cellulose-based polymer electrolytes, Cellulose 29 (2022) 8997–9034, https://doi.org/10.1007/ s10570-022-04834-w.
- [23] C. Yang, Q. Wu, W. Xie, X. Zhang, A. Brozena, J. Zheng, M.N. Garaga, B.H. Ko, Y. Mao, S. He, Y. Gao, P. Wang, M. Tyagi, F. Jiao, R. Briber, P. Albertus, C. Wang, S. Greenbaum, Y.Y. Hu, A. Isogai, M. Winter, K. Xu, Y. Qi, L. Hu, Copper-coordinated cellulose ion conductors for solid-state batteries, Nature 598 (2021) 590–596, https://doi.org/10.1038/s41586-021-03885-6.
- [24] D. Wang, H. Xiea, Q. Liu, K. Mu, Z. Song, W. Xu, L. Tian, C. Zhu, J. Xu, Low-cost, high-strength cellulose-based quasi-solid polymer electrolyte for solid-state lithium-metal batteries, Angew. Chem. Int. Ed. 62 (2023) e202302767, https://doi.org/10.1002/anje.202302767.
- [25] Y. Ogawa, H. Hidaka, S. Kimura, U.-J. Kim, S. Kuga, M. Wada, Formation and stability of cellulose-copper–NaOH crystalline complex, Cellulose 21 (2013) 999–1006, https://doi.org/10.1007/s10570-013-9977-4.
- [26] A.D. French, Increment in evolution of cellulose crystallinity analysis, Cellulose 27 (2020) 5445–5448, https://doi.org/10.1007/s10570-020-03172-z.
- [27] H. Fan, M. Li, E. Wang, Anion-functionalized interfacial layer for stable Zn metal anodes, Nano Energy 103 (2022) 107751.
- [28] Z. Tian, Y. Zou, G. Liu, Y. Wang, J. Yin, J. Ming, H.N. Alshareef, Electrolyte solvation structure design for sodium ion batteries, Adv. Sci. 9 (2022) 2201207, https://doi.org/10.1002/advs.202201207.
- [29] L. Hu, J. Deng, Y. Lin, Q. Liang, B. Ge, Q. Weng, Y. Bai, Y. Li, Y. Deng, G. Chen, X. Yu, Restructuring electrolyte solvation by a versatile diluent toward beyond

- 99.9% coulombic efficiency of sodium plating/stripping at ultralow temperatures, Adv. Mater. 36 (2024) 2312161, https://doi.org/10.1002/adma.202312161.
- [30] Y. Wang, H. Lan, S. Dong, Q. Zhu, L. Cheng, H. Wang, J. Wang, S. Wang, M. Tang, K.M. Shodievich, G. Wang, H. Wang, A high-power rechargeable sodium-ion full battery operating at -40 °C, Adv. Funct. Mater. 34 (2024) 2315498, https://doi.org/10.1002/adfm.202315498.
- [31] Z.E.M. Reeve, C.J. Franko, K.J. Harris, H. Yadegari, X. Sun, G.R. Goward, Detection of electrochemical reaction products from the sodium–oxygen cell with solid-state ²³Na NMR spectroscopy, J. Am. Chem. Soc. 139 (2017) 595–598, https://doi.org/ 10.1021/jacs.6b11333.
- [32] X. Zhan, M. Li, X. Zhao, Y. Wang, S. Li, W. Wang, J. Lin, Z.-A. Nan, J. Yan, Z. Sun, H. Liu, F. Wang, J. Wan, J. Liu, Q. Zhang, L. Zhang, Self-assembled hydrated copper coordination compounds as ionic conductors for room temperature solid-state batteries, Nat. Commun. 15 (2024) 1056, https://doi.org/10.1038/s41467-024-45372-2
- [33] M. Shakourian-Fard, G. Kamath, K. Smith, H. Xiong, S.K.R.S. Sankaranarayanan, Trends in Na-ion solvation with alkyl-carbonate electrolytes for sodium-ion batteries: insights from first-principles calculations, J. Phys. Chem. C 119 (2015) 22747–22759, https://doi.org/10.1021/acs.jpcc.5b04706.
- [34] J. Li, S. Sui, X. Zhou, K. Lei, Q. Yang, S. Chu, L. Li, Y. Zhao, M. Gu, S. Chou, S. Zheng, Weakly coordinating diluent modulated solvation chemistry for high-performance sodium metal batteries, Angew. Chem. Int. Ed. 63 (2024) e202400406, https://doi.org/10.1002/anie.202400406.
- [35] H. Yang, Q. Zhang, M. Chen, Y. Yang, J. Zhao, Unveiling the origin of air stability in polyanion and layered-oxide cathode materials for sodium-ion batteries and their practical application considerations, Adv. Funct. Mater. 34 (2023) 2308257, https://doi.org/10.1002/adfm.202308257.
- [36] Z. Gu, X. Zhao, K. Li, J. Cao, X. Wang, J. Guo, H. Liu, S. Zheng, D. Liu, H. Wu, X. Wu, Homeostatic solid solution reaction in phosphate cathode: breaking high-voltage barrier to achieve high energy density and long life of sodium-ion batteries, Adv. Mater. 36 (2024) 2400690, https://doi.org/10.1002/adma.202400690.
- [37] W. Li, H. Li, J. Liu, S. Lin, Q. Chen, W. Ji, Z. He, P. Zhang, J. Zhao, Systematic safety evaluation of quasi-solid-state lithium batteries: a case study, Energy Environ. Sci. 16 (2023) 5444–5453, https://doi.org/10.1039/D3EE03073C.